On Sea Surface Roughness Parameterization and Its Effect on Tropical Cyclone Structure and Intensity

Zhihua Zeng *

Shanghai Typhoon Institute, Laboratory of Typhoon Forecast Technique/CMA, Shanghai, China

Yuqing Wang

International Pacific Research Center and Department of Meteorology, School of Ocean and Earth Science and Technology, University of Hawaii at Manoa, Honolulu, HI 96822

Yihong Duan

National Meteorological Center, China Meteorological Administration, Beijing, China

Lianshou Chen

Chinese Academy of Meteorological Sciences, China Meteorological Administration, Beijing, China

December 18, 2008 (Submitted)

April 10, 2009 (Revised)

Dateline

Revised for ***Advances in Atmospheric Sciences***

* Corresponding author address: Zhihua Zeng, Shanghai Typhoon Institute, 166 Puxi Road, Shanghai 200030, China. E-mail: zengzh@mail.typhoon.gov.cn

Abstract

A new parameterization scheme of sea surface momentum roughness length for all wind regimes including high winds under tropical cyclone (TC) conditions, is constructed based on measurements from Global Positioning System (GPS) dropsonde. It reproduces the observed regime transition, namely, an increase of the drag coefficient with the increase of wind speed up to 40 m s^{-1} followed by a decrease with further increase of wind speed.

The effect of this parameterization on the structure and intensity of tropical cyclones is evaluated using TCM4. The results show that the final intensity is increased by 10.5% (8.9%) in the maximum surface wind speed and by 8.1 hPa (5.9 hPa) increase in the minimum sea surface pressure drop with (without) dissipative heating. This intensity increase is found to be mainly due to the reduced frictional dissipation in the surface layer and with little to do with either the surface enthalpy flux or latent heat release in the eyewall convection. The effect of the new parameterization on the storm structure is found to be insignificant and occur only in the inner core region with the increase in tangential winds in the eyewall and the increase in temperature anomalies in the eye. This is because the difference in drag coefficient appears only in a small area under the eyewall. Implications of the results are briefly discussed.

Keywords: Sea surface roughness, TC structure and intensity, Drag coefficient, Numerical model

1. Introduction

The classic Monin-Obukhov similarity theory, which predicts logarithmic wind profiles in the lowest several hundred meters of the atmosphere, is widely used in atmospheric models to parameterize surface turbulent fluxes of momentum, heat, and moisture with the model resolvable variables that drive and are influenced by the fluxes. Although a lot of efforts have been made to refine the flux parameterizations for several decades, uncertainties still remain in the specification of the parameters, such as the roughness lengths for momentum, heat and moisture used in the parameterization schemes, affecting the calculation of both drag and exchange coefficients. These parameters are obtained by calibration with measurements over the ocean only available for winds less than 25 m s^{-1} (Liu et al. 1979; Smith 1988), which corresponds to weak tropical storms. In practice, these parameters are extrapolated to higher wind speeds in most atmospheric models, including those used for tropical cyclones (Kurihara et al. 1998; Bao et al. 2000; Wang 2001, 2002a). Such an extrapolation is necessary because there have been no sufficient direct measurements available to determine these parameters at high wind speeds.

The uncertainty in calculating the surface fluxes is believed to be one of the major factors that limit the predictability of tropical cyclone (TC) intensity (Wang and Wu 2004) since surface fluxes of momentum and enthalpy are vital to the development and maintenance of tropical cyclones (Malkus and Riehl 1960; Ooyama 1969). Emanuel (1995) and Bister and Emanuel (1998) showed that the maximum potential intensity (MPI) of a tropical cyclone is directly proportional to the square root of the ratio of exchange coefficient (C_h) to drag coefficient (C_d) at the ocean surface $[(C_h/C_d)^{1/2}]$ under the eyewall,

$$V_{\max} = \sqrt{\frac{C_h}{C_d}\frac{T_s - T_0}{T_0}(k_0^* - k)}, \qquad (1)$$

where V_{max} is the maximum surface wind, C_h the exchange coefficient, C_d the drag coefficient, T_s sea surface temperature, T_0 outflow layer temperature, k_0^* and k are the enthalpy of saturated air at sea surface temperature and the enthalpy of air near the ocean surface, respectively. Emanuel proposed that the ratio C_h/C_d must be larger than three-fourths in real TCs; otherwise the wind speeds would be much weaker than the observed.

The drag and exchange coefficients at high wind speeds can be affected significantly by ocean waves and sea spray since the classic Monin-Obukhov similarity theory does not explicitly take into account the full physics of the surface waves and sea pray. Although there have been some efforts considering these effects in recent years (Andreas and Emanuel 2001; Wang et al. 2001; Andreas 2004), it is still hard to make any significant progress because of the great difficulty in direct measurements at extremely high wind conditions.

Based on scaling arguments, Emanuel (2003) proposed that in the limit of very high wind speed, the air-sea transition layer would become self-similar, permitting deductions of air-sea exchange. He hypothesized that drag coefficient based on the gradient wind speed should become independent of wind speed in the high wind limit. However, it is not clear at what wind speed the drag coefficient becomes independent of wind speed.

The results from laboratory experiments suggest that the drag coefficient start to decrease with the increase of wind speed as 10-m height wind speed exceeds 25 m s^{-1} (Alamaro et al. 2002). This reduction tendency has recently been verified by Powell et al. (2003) based on the Global Positioning System (GPS) dropwindsonde data, but with the transition occurring at 10-m height wind speed of about 40 m s^{-1} instead of 25 m s^{-1} found in the laboratory experiments

by Alamaro et al. (2002). The laboratory experiments by Donelan et al. (2004) show that the drag coefficient reaches a saturation point at high wind speeds greater than about 33 m s^{-1}. The above results from laboratory experiments are supported by the airborne turbulence flux measurements from CBLAST-Hurricane field experiments in the North Atlantic (Drennan et al. 2007; French et al. 2007). The behavior of the C_d at high wind speeds was also found in theoretical studies by Emanuel (2003) and Makin (2005). On the other hand, the first measurements of enthalpy flux in the CBLAT-Hurricane boundary layer show that the exchange coefficient is almost independent of wind speed (Dreennan et al. 2007; Zhang et al. 2008).

A possible physical explanation for the transition of the drag coefficient is the development of a sea foam layer at the air-sea interface (Powell et al. 2003). As surface winds exceed 40 m s^{-1}, the sea surface becomes completely covered by a layer of foam, which impedes the transfer of momentum from the atmosphere to the ocean, leading to a weakly increase of friction velocity and a decrease of drag coefficient with increasing wind speed (vertical bars in Fig. 1). Recently, Moon et al. (2004a,b,c) used a coupled wave–wind (CWW) model to show that the drag coefficient levels off (or even decreases) at wind speeds exceeding 30 m s^{-1}. This finding is significant in advancing our understanding of the air-sea interaction in high wind regimes, provides the first observation for verification of surface layer parameterizations, and thus can improve TC intensity forecasts by numerical weather prediction models (Wang and Wu 2004).

Although the drag coefficient is negative to the intensity of TCs, its induced dissipative heating could be positive. Previous studies have showed that the dissipative heating can be large in tropical cyclones when the wind speeds exceed 40 m s^{-1} and increases the tropical

cyclone intensity by 10-20% in the maximum surface wind (Bister and Emanuel 1998; Zhang and Altshuler 1999). Bister and Emanuel (1998) found that the dissipative heating, which had always been neglected in earlier numerical TC models and theoretical analysis of the TC MPI, can have a positive contribution to the tropical cyclone intensity. They showed in both theoretical and numerical models that the maximum wind speed of a tropical cyclone would be increased by roughly 20% with the inclusion of dissipative heating. Zhang and Altshuler (1999) investigated the effect of dissipative heating on the intensity of Hurricane Andrew (1992), using a 72-h simulation with the mesoscale model version 5 (MM5) of the Pennsylvania State University-National Center for Atmospheric Research (PSU-NCAR). Their results confirmed the conclusion of Bister and Emanuel (1998) that the inclusion of dissipative heating can increase the hurricane intensity by 10% in the maximum surface wind at the most intense period when surface wind exceeds 70 m s^{-1}. Therefore when we try to evaluate the effect of drag coefficient on the intensity of tropical cyclones, it is necessary to isolate the possible opposite effect due to dissipative heating.

In this study, we first construct a parameterization scheme for sea surface roughness length. This parameterization predicts an increase of drag coefficient with increasing wind speed up to about 40 m s^{-1}, and then a decrease with increasing wind speed, as suggested by recent theoretical studies of Emanuel (2003) and Mankin (2005) and results from laboratory experiments of Alamaro et al. (2002) and measurements from Global Positioning System (GPS) dropsonde of Powell et al. (2003), Drennan et al. (2007), French et al. (2007). The effect of this parameterization on TC intensity and structure is evaluated using a newly developed, fully-compressible, nonhydrostatic primitive equation model (TCM4). For this purpose, the results from the traditional and the new parameterizations with and without dissipative heating

in TCM4 are analyzed and compared in this study.

The rest of the paper is organized as follows. The next section presents the construction of a new parameterization scheme for sea surface roughness length applicable to all wind regimes. Section 3 describes the tropical cyclone model (TCM4) used and the design of numerical experiments. The results from different experiments are analyzed and compared in section 4 to elucidate the effect of the new parameterization scheme on the structure and intensity of the simulated tropical cyclones and the contribution to the difference in storm structure and intensity by dissipative heating. Conclusions are drawn in the last section.

2. Sea Surface Roughness Parameterization

In most applications, the sea surface roughness length for momentum (z_u in meter) is specified by the Charnock's (1955) expression plus a smooth flow limit (Smith 1988):

$$z_u = \frac{\alpha u_*^2}{g} + \frac{0.11\nu}{u_*}, \tag{2}$$

where ν is the molecular viscosity of air, g the gravitational acceleration, u_* the friction velocity, and α the Charnock parameter, which is a constant in the range of 0.011-0.035 in practical applications (Large and Pond 1982; Smith 1988). In a recent study, Fairall et al. (2003) allowed the Charnock parameter α to vary with wind speed

$$\alpha = \begin{cases} 0.011 & for \quad U_{10} \le 10 ms^{-1} \\ 0.011 + 0.000875(U_{10} - 10) & for \quad 10 < U_{10} < 18 ms^{-1} \\ 0.018 & for \quad U_{10} \ge 18 ms^{-1} \end{cases} \tag{3}$$

where U_{10} is the scalar wind speed including the convective gustiness at 10-m height (Fairall et al. 2003). Fairall et al. (2003) showed that the wind-dependent Charnock parameter fits better the available observations up to wind speed of about 25 m s^{-1}. Note that in most numerical

weather prediction or climate models, the Charnock parameter is usually set to be a constant, independent of wind speed.

It remains unclear whether the Charnock parameter given in (3) is applicable to wind speed higher than 25 m s^{-1}, which corresponds to high winds under severe weather systems, such as tropical cyclones. The Charnock relation (2) with the Charnock parameter in (3) predicts a monotonic increase of the momentum roughness length, friction velocity, and 10-m height drag coefficient with increasing wind speed at neutral condition (Fig. 1). This is widely used in most atmospheric models, while it is contrary to the latest analysis of the GPS dropsonde data by Powell et al. (2003), who showed an increase of roughness length and drag coefficient up to wind speed of about 40 m s^{-1}, but followed by a decrease as wind speed further increases (Fig. 1). This indicates that the constant Charnock parameter of 0.018 is too large at very high wind speeds, and that the Charnock parameter should be wind-dependent for wind speeds greater than 25 m s^{-1}.

To better fit the roughness length, friction velocity, and drag coefficient to observations, we constructed a parameterization scheme for the Charnock parameter, which can be applied to high wind speeds. Instead of a constant Charnock parameter for wind speeds greater than 18 m s^{-1} in (3), we allow the Charnock parameter to be a function of friction velocity for wind speeds greater than 25 m s^{-1}. The equation (3) is thus modified to

$$\alpha = \begin{cases} 0.011 & for \quad U_{10} \le 10 ms^{-1} \\ 0.011 + 0.000875(U_{10} - 10) & for \quad 10 < U_{10} < 18 ms^{-1} \\ 0.018 & for \quad 18 \le U_{10} \le 25 ms^{-1} \\ \max\left\{ 2.0 \times 10^{-3}; \dfrac{0.018}{1 + \delta(u_* - u_{*25})^2 - \gamma(u_* - u_{*25})^{1.6}} \right\} & for \quad U_{10} > 25 ms^{-1} \end{cases} \tag{4}$$

where u_{*25} is the friction velocity at scalar wind speed of 25 m s^{-1}, δ and γ are two constants,

which are tunable parameters. Our initial evaluation suggests their values be between 0.3-1.0 for δ and 0.05-0.75 for γ to give the roughness length, friction velocity, and drag coefficient comparable to the analysis of Powell et al. (2003). Note that we are conservative in our parameterization and set δ = 1.0, γ = 0.6 and thus allow the flux parameters to be at the 95% confidence upper limits of the corresponding observations (Fig. 1). A lower bound of Charnock parameter in (4) is set for high wind speed so that the drag coefficient is not allowed to be less than 0.002 for winds greater than 65 m s^{-1} (Fig. 1). Another reason for us to choose these parameters is based on the fact that Powell et al. (2003) seemed to underestimate the surface roughness length (and surface drag coefficient, see below) for wind speeds less than 25 m s^{-1} (Fig. 1). To have a smooth regime transition, we do not completely follow Powell et al.'s estimation but we do follow the trend given in their study. The roughness length for heat and moisture is calculated based on Fairall et al. (2003)

$$z_T = z_q = \min(1.1\times10^{-4}, \quad 5.5\times10^{-5} R_r^{-0.6}), \tag{5}$$

where R_r is the roughness Reynolds number, defined as $R_r = \frac{u_* z_u}{\nu}$. This relationship gives a linkage between the roughness length for heat/moisture and that for momentum through the roughness Reynolds number, a measure of the intensity of surface turbulence. Note that although Fairall et al. (2003) parameterization (5) was obtained for weak and moderate intense winds, its explicit dependence on the roughness Reynolds number indicates that this parameterization could be used for high wind regimes as well. We will show later that (5) produces the exchange coefficient under hurricane wind conditions comparable to the latest measurements of enthalpy flux in the CBLAST-Hurricane boundary layer experiment (Dreennan et al. 2007; Zhang et al. 2008).

Since the roughness length is a function of the friction velocity, which in turn is a function of roughness length, iteration is thus necessary in order to obtain the drag coefficient. For example, under neutral surface conditions, the Monin-Obukhov similarity theory predicts a logarithmic relation between the wind speed and height. For 10 m height, the wind can be written as:

$$U_{10} = (u_* / \kappa)[\ln(10 / z_u)], \tag{6}$$

Here, $u_* = (\tau / \rho)^{1/2}$ is the friction velocity, $\kappa = 0.4$ the von Karman constant, ρ the air density of the air, τ the wind stress determined by the bulk aerodynamic formula:

$$\tau = \rho C_d U_{10}^2, \tag{7}$$

After some manipulations, we can obtain the drag coefficient and friction velocity as:

$$\begin{cases} C_d = [\dfrac{k}{\ln(10 / z_u)}]^2 \\ u_* = \sqrt{C_d} U_{10} \end{cases}, \tag{8}$$

Given the first guess of any one of the three parameters (z_u, u_*, C_d), using (2) and (8) with either (3) or (4), we can obtain the three parameters by iteration. Since the first guess can be obtained from the previous time step in the numerical model, 3-4 iterations can thus give quite accurate results.

The corresponding drag coefficient and exchange coefficient at neutral conditions as a function of 10-m height wind speed based on the new parameterization (4) and the traditional one (3) are compared in Fig. 1. We can see that the new scheme produces the decreasing trends for both the drag and exchange coefficients for wind speeds greater than 40 m s^{-1}, consistent with the observational results for drag coefficient by Powell et al. (2003) and French et al. (2007) and the measurements for exchange coefficient in the CBLAT-Hurricane boundary

layer experiment by Dreennan et al. (2007) and Zhang et al. (2008).

Zhang et al. (2008) showed that the exchange coefficient in hurricane boundary layer is almost independent of wind speed and has a mean value about 1.2×10^{-3}. With the use of (5), we also got the similar value for the exchange coefficient (Fig. 1c). The parameter $(C_h/C_d)^{1/2}$ decreases with wind speed in the traditional parameterization and becomes less than 0.6 for wind speeds larger than 55 m s^{-1} (Fig. 1d). With the new scheme, however, this parameter slightly increases with wind speed for winds larger than 40 m s^{-1} and reaches a constant of 0.76 for winds greater than 65 m s^{-1}. This is again consistent with the latest of Drennan et al. (2007, see their Fig. 11) and Zhang et al. (2008, see their Fig. 4). Therefore the new parameterization scheme appears to be supported by the results from CBLAST measurements. However, we should point out that even though our parameterized drag and change coefficients are comparable to recent results from field measurements, observations, in particular for the exchange coefficient, were still limited to wind speed up to about 30 m s^{-1} (Drennan et al. 2007; Zhang et al. 2008). Therefore there are still uncertainties for the parameterization of the exchange coefficient under hurricane wind conditions, including the effect of sea spray. Nevertheless, our focus is mainly on the effect of drag coefficient on the TC structure and intensity in idealized simulations, it is hoped that the uncertainties in the exchange coefficient would not alter our main conclusions from this study.

3. Model Description and Experimental Design

a. Model description

The model used in this study is the fully compressible, nonhydrostatic, primitive equation model – TCM4. It is an extension of the previously developed hydrostatic model TCM3 (Wang

1999, 2001, 2002a) with the replacement of the hydrostatic dynamical core by a fully-compressible, nonhydrostatic dynamical core. A major feature of TCM4 is its capability of simulating the inner-core structure and the associated intensity change of a tropical cyclone at nearly cloud resolving resolution. The use of multiply nesting and automatic mesh movement in TCM4 allows us to use adequate medium sizes for meshes with fine resolutions so that we can save computer time. A full description of TCM4 can be found in Wang (2007). Here only the major features of the model are highlighted.

TCM4 shares the state-of-the-art model physics, the two-way interactive multiple nesting, and automatic mesh movement with its hydrostatic counterpart TCM3. The model equations are formulated in the Cartesian coordinates in the horizontal and mass coordinate in the vertical. An efficient forward-in-time, explicit time splitting scheme, similar to the one described by Wicker and Skamarock (2002), is used for model integration with the fifth-order upwind scheme for horizontal advection, which takes into account the effect of spatial variation of the advective flow (Wang 1996). Note that the model has a flat surface with an unperturbed surface pressure of 1010 hPa. The model top is set at about 38 km and a sponge upper boundary condition similar to that used in Durran and Klemp (1983) is used to absorb the upward propagating sound and gravity waves.

The model physics include an E-ε turbulence closure scheme for subgrid scale vertical turbulent mixing; a modified Monin-Obukhov scheme for the surface flux calculation (Fairall et al. 2003); an explicit treatment of cloud microphysics package, which includes mixed-phase cloud processes (Wang 1999, 2001); a linear fourth-order horizontal diffusion for all prognostic variables except for that related to the mass conservation equation; and a simple Newtonian cooling term is added to the potential temperature equation to mimic the radiative cooling in

the model as used in TCM3 and in Rotunno and Emanuel (1987); dissipative heating due to molecular friction, which is included by adding the turbulent kinetic energy dissipation rate (ε) into the thermodynamic equation (Wang 2001).

The model domain is multiply nested with two-way interactive nesting and with the inner meshes automatically moving following the model tropical cyclone as used in TCM3 (Wang 2001). As in Wang (2001), the same model physics are used in all meshes. Since no large-scale environmental flow is included in this study, convection is mainly active in the inner core region and in the spiral rainbands that are within about a radius of 200 km from the cyclone center and thus can be covered in the finest innermost domain. Therefore, cumulus parameterization is not considered even in the two outermost coarse meshes in this study. In our current model settings, the model domain is quadruply nested with resolutions of 67.5, 22.5, 7.5, 2.5 km for the four meshes, respectively. The model has 26 σ levels in the vertical with vertically staggered grid such that horizontal winds, perturbation pressure and potential temperature and all moist variables are located at the integer levels while the vertical wind and turbulent kinetic energy and its dissipation rate are arranged at the half levels. As in Wang (2001, 2007), the same model physics are used in all mesh domains.

b. Experimental design

The experimental design follows Wang (2001, 2007). The model is initialized with an axisymmetric cyclonic vortex on an *f*-plane of 18^{o}N in a quiescent environment over the ocean with a constant sea surface temperature of 29^{o}C. The initial thermodynamic structure of the unperturbed model atmosphere is defined as the western Pacific clear-sky environment given by Gray et al. (1975). The tangential wind of the initial cyclonic vortex is defined by

$$V_T(r,\sigma)=\begin{cases} V(r)\sin\left[\dfrac{\pi}{2}\left(\dfrac{\sigma-\sigma_T}{1-\sigma_T}\right)\right], & \sigma>\sigma_u; \\ 0, & \sigma\le\sigma_u; \end{cases} \tag{9}$$

where $\sigma_u = 0.15$ and

$$V(r)=\begin{cases} V_m\left(\dfrac{r}{r_m}\right)\left\{\exp\dfrac{1}{b}\left[1-\left(\dfrac{r}{r_m}\right)^b\right]-\dfrac{|r-r_m|}{R_o-r_m}\exp\dfrac{1}{b}\left[1-\left(\dfrac{R_o}{r_m}\right)^b\right]\right\}, & r\le R_o; \\ 0, & r>R_o; \end{cases} \tag{10}$$

where V_m is the maximum tangential wind at the radius r_m, r the radius, b is a non-dimensional parameter which determines the rate of radial decay of tangential wind outside the radius of maximum wind, and R_o the radius out of which the vortex wind vanishes. The mass and thermodynamic fields associated with the vortex are obtained by solving the nonlinear balance equation as described in the Appendix of Wang (2001). In all numerical experiments discussed in this study, we set V_m = 25 m s^{-1}, r_m = 80 km, R_0 = 900 km, and b = 1.0. This initial vortex wind profile is the same as that used in Wang (2007).

To evaluate the effect of different sea surface roughness length parameterizations on the simulated tropical cyclone structure and intensity, we have performed four experiments (Table 1). In the first two experiments, dissipative heating is included, one (CTL_DH) with the traditional momentum roughness parameterization (Fairall et al. 2003) and the other (NEW_DH) with the new parameterization using the Charnock parameter given in (4). The second two experiments (CTL_noDH and NEW_noDH) are similar to the first ones but with the dissipative heating turned off to allow an examination of the opposite effect due to dissipative heating with different surface roughness parameterizations by comparison with the results from the first two experiments. The roughness length for heat and moisture is calculated with (5) in all four experiments. Note that the exchange coefficients are slightly different in the

four experiments due to the dependence of the roughness length itself on the friction velocity through the roughness Reynolds number (5) and the dependence of exchange coefficient on the friction velocity as well (Fig. 1). The model is integrated up to 216 h for all experiments.

4. Results

a. Storm intensity

Figure 2 shows the evolution of the maximum wind speed at the lowest model level about 35.6 m above the sea surface and the minimum central sea surface pressure in the four experiments. Regardless with (CTL_DH and NEW_DH) or without (CTL_noDH and NEW_coDH) dissipative heating, there is little difference in the intensification rate up to about 48 h of simulation before the maximum surface wind exceeds about 40 m s^{-1} (or about 50 m s^{-1} for the lowest model level maximum wind). This is what we should expect since there is little difference in the new and the traditional surface roughness parameterizations for surface winds lower than 40 m s^{-1} (Fig. 1). Differences between the storm intensification rates in different experiments become visible after 48–60 h of simulation when the maximum surface wind exceeds 40 m s^{-1}. The storm intensifies at a relatively higher rate up to about 96-120 h of simulation with the new surface roughness parameterization (NEW_DH and NEW_noDH) than with the traditional one (CTL_DH and CTL_noDH). As a result, the storm is always stronger at its mature stage in the experiment with the new surface roughness parameterization (Fig. 2). Furthermore, with the same surface roughness parameterization, storms are generally stronger when the dissipative heating is included (CTL_DH versus CTL_noDH and NEW_DH versus NEW_noDH).

Table 1 gives the mean intensity of the model storms averaged between 144h and 216 h during which the storms reached their quasi-steady evolution in the four experiments. We can see that the maximum wind at the lowest model level is about 10.5% (8.9%) stronger in NEW_DH (NEW_noDH) than in CTL_DH (CTL_noDH), namely, 81 m s^{-1} versus 73.3 m s^{-1} (76.9 m s^{-1} versus 70.6 m s^{-1}). The minimum central sea surface pressure is about 8.1 hPa (5.9 hPa) deeper in NEW_DH (NEW_noDH) than in CTL_DH (CTL_noDH), namely, 905.9 hPa versus 914.0 hPa (914.4 hPa versus 920.3 hPa). The increase in the storm intensity due to the use of the new surface roughness parameterization compared to the traditional one is enlarged by about 18% in the maximum surface wind (8.9% versus 10.5%) and 37% in the minimum sea surface pressure (5.9 hPa versus 8.1 hPa) due to the inclusion of dissipative heating. This is consistent with the fact that dissipative heating increases with the cube of wind speed, and thus its positive effect on storm intensity would be more significant for stronger storms. This is a positive feedback to the intensity difference between the experiments with and without dissipative heating.

From Table 1, we can also see that dissipative heating increases the storm intensity by 5.3% in the maximum surface wind in the experiments with the new surface roughness parameterization (81.0 m s^{-1} in NEW_DH versus 76.9 m s^{-1} in NEW_noDH), but only by 3.8% in the experiments with the traditional one (73.3 m s^{-1} in CTL_DH versus 70.6 m s^{-1} in CTL_noDH). Consistent with the increase in the maximum surface wind, the minimum sea surface pressure is 8.5 hPa (6.3 hPa) deeper if the new parameterization (traditional one) is used. The increase in the maximum surface wind due to dissipative heating is smaller than that found in both Bister and Emanuel (1998) and Zhang and Altshuler (1999). Bister and Emanuel reported an increase of about 20% in the MPI by dissipative heating, while Zhang and Altshuler

found a 10% increase in the maximum surface wind in a model when surface wind exceeds 70 m s^{-1}. The smaller percentage in this study is mainly due to the fact that the storms in our model are weaker than those studied by Bister and Emanuel (1998) and Zhang and Altshuler (1999), because the effect of dissipative heating on tropical cyclone intensity increases with the increase in storm intensity.

b. Surface flux parameters

Figure 3 shows the radial profiles of the azimuthal mean 10-m height wind speed and rainfall rate averaged between 144 and 216 h of simulation in the four experiments listed in Table 1. Consistent with the increase in the maximum wind speed at the lowest model level given in Fig. 2, the azimuthal mean 10-m height wind speed with the new surface roughness parameterization (NEW_DH/NEW_noDH) is stronger than that with the traditional parameterization (CTL_DH/CTL_noDH) only under the eyewall region between radii 20 and 50 km from the storm center. This is the case because the wind speeds are larger than 40 m s^{-1} only in a small area under the eyewall (Figs. 3a and 3c). This indicates that the use of the new surface roughness parameterization only increases the inner core intensity of the model tropical cyclone and has little effect on the wind strength of the storm outside the core. The intensity increase with the new surface roughness parameterization could not be explained by the latent heat release associated with eyewall convection since the azimuthal mean rainfall rates in the experiments with the new parameterization (NEW_DH/NEW_noDH) and with the traditional one (CTL_DH/CTL_noDH) are almost the same. This implies that the intensity difference in the simulated storms stems predominantly from the surface processes.

Figure 4 shows the azimuthal mean surface momentum roughness length and surface

friction velocity averaged between 144-216 h of simulation in the four experiments listed in Table 1. The surface roughness length in NEW_DH (NEW_noDH) is greatly reduced under the eyewall compared to that in CTL_DH (CTL_noDH) (Figs. 4a, 4c). This is what we should expect given its parameterization discussed in section 2. The new surface roughness length decreases with increasing wind speed as surface wind exceeds 40 m s^{-1} (Fig. 1b). This occurs only between radii 15 and 50 km under the eyewall (Figs. 4a, and 4c). Since the friction velocity increases with wind speed at a smaller rate with the new surface roughness parameterization than with the traditional one when the surface wind exceeds 40 m s^{-1} (Fig. 1a), it is thus smaller in NEW_DH (NEW_noDH) than in CTL_DH (CTL_noDH) under the eyewall where the local surface winds are larger than 40 m s^{-1} (Figs. 4b and 4d).

The reduced momentum roughness length at high wind speeds is responsible for a 35% reduction in surface drag coefficient (C_d) and a 10% reduction in surface exchange coefficient (C_h) under the eyewall in NEW_DH (NEW_noDH) relative to that in CTL_DH (CTL_noDH) (Figs. 5a, 4c). As a result, the parameter $(C_h/C_d)^{1/2}$ increases by 14.8% (12.5%) in NEW_DH (NEW_noDH) at the radius of maximum wind (20 km from the storm center) relative to that in CTL_DH (CTL_noDH). This increase in parameter $(C_h/C_d)^{1/2}$ is not in proportion to the intensity increase shown in Fig.2 and listed Table 1 as inferred from the theoretical MPI given in Eq. (1) developed by Emanuel (1995, see also Bister and Emanuel 1998). We, however, note that this parameter is not a constant under the eyewall region. If an area average between 15 and 40 km from the storm center is made, the increase in $(C_h/C_d)^{1/2}$ will be 8.3% (7.3%) for the new roughness parameterization in NEW_DH (NEW_noDH) relative to traditional one in CTL_DH (CTL_noDH). This is closer to the intensity increase of 10.5% (8.9%) in NEW_DH (NEW_noDH). Part of the difference can be explained by the dependence of the surface

enthalpy deficit (k_o^*-k) in Eq. (1), which increases with the deepening of sea surface pressure due to a given constant sea surface temperature. However, this positive feedback seems not to increase the enthalpy flux at the ocean surface due to partial offsetting by the decrease in surface exchange coefficient (Figs. 5a and 5c). As we see from Fig. 6, the exact enthalpy flux with the new surface flux parameterization in NEW_DH (NEW_noDH) has little difference from that in CTL_DH (CTL_noDH). This excludes any direct thermodynamic contributions to the intensity increase with the new surface roughness parameterization in the model. Note that the new surface roughness parameterization gives the surface exchange coefficient nearly a constant of 0.0011-0.0012 (Figs. 5b and 5c), which is very close to that obtained from recent observations in real hurricanes over the North Atlantic (Black et al. 2007, Drennan et al. 2007; Zhang et al. 2008).

The only contribution to the intensity increase with the new surface roughness parameterization, therefore, is the decrease in the dynamical dissipation at the ocean surface. One of the measures for the dynamical dissipation is the surface wind stress. Figure 6 shows the corresponding wind stresses from the four experiments. Similar to other surface parameters, the difference in surface wind stress occurs also mainly under the eyewall. Consistent with the decrease in surface drag coefficient (Fig. 5) with the new surface roughness parameterization, the surface wind stress is reduced considerably under the eyewall with the maximum reduction near the radius of maximum wind. This proportional decrease in surface dissipation seems to be a major player for the intensity increase with the new surface roughness parameterization (Fig. 2 and Table 1). Therefore, we conclude that it is the reduced dissipation that is responsible for the intensity increase in NEW_DH (NEW_noDH) compared to CTL_DH (CTL_noDH).

c. Storm structure

The remained question we hope to address is whether the surface roughness parameterization can cause any changes in the overall structure of the simulated tropical cyclone in the model. Figure 7 gives the axisymmetric structure of the model tropical cyclone averaged between 144 and 216 h of simulation in CTL_DH, including the tangential and radial winds, vertical velocity, temperature anomalies, potential vorticity (PV), and the kinetic energy of asymmetric flow (or eddy kinetic energy, EKE). The storm has its maximum tangential wind at a radius of about 20 km (Fig. 7a), a shallow inflow layer in the lowest atmospheric boundary layer and a relatively deep outflow layer in the upper troposphere (Fig. 7b). The eyewall ascent tilts radially outward with height (Fig. 7c). The storm has a warm-cored structure in the mid-upper troposphere with the maximum temperature anomaly of 16^{o}C (Fig. 7d) and an off-centered PV maximum just within the radius of maximum wind (Fig. 7e). This PV structure satisfies the necessary condition for barotropic instability and thus is dynamically unstable to small perturbations, favoring the formation of asymmetric eddies in the eyewall as identified as vortex Rossby waves as discussed in Montgomery and Kallenbach (1997), Montgomery and Lu (1997), Montgomery and Enagonio (1998), Montgomery and Brunet (2002), Chen and Yau (2001), and Wang (2001, 2002b, c). As a result, the eddies (or vortex Rossby waves) are generally active in the eyewall region with an outward tilt with height in the simulated storm, especially in the mid-lower troposphere, as seen in Fig. 7f for the azimuthal mean eddy kinetic energy.

The axisymmetric structure of the storm simulated in NEW_DH with the new surface roughness parameterization (Fig. 8) is quite similar to that in CTL_DH shown in Fig. 7. Consistent with the surface parameters discussed earlier, the major difference in storm structure between NEW_DH and CTL_DH is in the eyewall region. As we can see from the difference

fields in Fig. 9 (NEW_DH minus CTL_DH), the tangential wind is increased mainly in the inner side of the eyewall throughout the troposphere (Fig. 9a). Although the storm in NEW_DH is stronger than that in CTL_DH), the difference in the secondary circulation (radial-vertical circulation) is insignificant (Figs. 9b and 9c). The temperature anomaly in the inner core is about 2^{o}C warmer in NEW_DH than in CTL_DH (Fig. 9d), consistent with the increased vertical shear of tangential wind, especially in the upper troposphere in the eyewall (Fig. 9a), and the stronger storm in the former than in the latter (Fig. 2a). In response to the increased tangential wind in the eyewall, the PV is increased in the mid-lower troposphere but reduced in the upper troposphere within the radius of maximum wind (Fig. 9e). Eddies seem to be more active in the mid-upper troposphere in NEW_DH than that in CTL_DH (Fig. 9f), consistent with the increased PV gradient across the eyewall (Figs. 7e, 8e and 9e), which could support more active vortex Rossby waves in the eyewall.

As already mentioned earlier (see Table 1), the reduced surface drag coefficient may reduce the dissipative heating in NEW_DH compared to that in CTL_DH. This indeed is the case as we can see from Fig. 10. The maximum dissipative heating near the surface is about 8 K h^{-1} in CTL_DH (Fig. 10a) and 6 K h^{-1} in NEW_DH (Fig. 10b), giving rise to a reduction of about 25% in the later. Therefore, the difference in this dynamical heating also contributes to the reduced intensity increase in NEW_DH relative to CTL_DH as inferred from the theoretical MPI given in (1). Note that the magnitude and distribution of dissipative heating rate and its effect on the storm intensity are all comparable with the results of Bister and Emanuel (1998) although we used the TKE dissipation rate as the dissipative heating in TCM4. Without dissipative heating, the overall structure difference between NEW_noDH and CTL_noDH (Fig. 11) is similar to that between NEW_DH and CTL_DH (Fig. 9). In this case, however, the

differences in radial winds (Fig. 11b) and eyewall ascents (Fig. 11c) are larger while the difference in temperature anomaly is slightly smaller but occurs at a higher level (Fig. 11d) than those with dissipative heating (Fig. 9d). This comparison indicates that dissipative heating seems to act to reduce the structure difference of the model storms between the new and traditional surface roughness parameterizations.

Dissipative heating contributes to tropical cyclone intensity positively (Table 1 and see also Bister and Emanuel 1998; Zhang and Altshuler 1999), but it is not clear to what degree the dissipative heating may affect the tropical cyclone structure. As a byproduct of this study, the difference in the axisymmetric structure of the simulated storm averaged between 144 and 216 h of simulation in CTL-DH and CTL_noDH (Fig. 12) is examined. We can see from Fig. 12 that dissipative heating has a considerable effect on the inner core structure of the tropical cyclone. Its effect on the storm structure is considerably larger than that induced by the surface roughness parameterization shown in Figs. 9 and 11. Now, the increase in inner-core tangential winds is more aligned in the vertical (Fig. 12a) and does not follow the titled eyewall seen in Figs. 9 and 11, giving rise to a higher and stronger warm core in the upper troposphere (Fig. 12d). Further, the positive-negative couplets in vertical motion (Fig. 12c) and the radial winds (Fig. 12b) in the eyewall region manifest an inward shift of the eyewall as well as the radius of maximum wind due to the inclusion of dissipative heating. Similar structure difference is found between NEW_DH and NEW_noDH but the difference is smaller than that between CTL_DH and CTL_noDH due to the smaller dissipative heating with the new surface roughness parameterization (not shown).

5. Conclusions and discussion

Results from numerical and theoretical models indicate the sensitivity of the maximum intensity of tropical cyclones to the ratio of the enthalpy exchange coefficient to the momentum drag coefficient. Both the drag and exchange coefficients, however, are extrapolated from the low wind regimes based on limited observations up to wind speed of about 25 m s^{-1} in most tropical cyclone models. This extrapolation predicts a monotonic increase of drag coefficient as the wind speed increases. Recent observations from GPS dropsondes provide boundary layer winds under tropical cyclones. Analysis of these data shows a reduced drag coefficient for wind speeds higher than 40 m s^{-1} (Powell et al. 2003). In this study, based on these new observations, a parameterization scheme for the surface momentum roughness length is constructed, which can reproduce the observed regime transition and thus is applicable to all wind regimes, including the high winds under tropical cyclones.

The effect of the new parameterization on the structure and intensity of tropical cyclones is evaluated using a high-resolution tropical cyclone model. Since there is no difference between the new and the traditional schemes for wind speed less than 40 m s^{-1}, a relatively high constant sea surface temperature of 29^{o}C is used so that the model storm can intensify strong enough to allow a reasonable evaluation. The results show that although the intensification rate is little affected by the use of the new parameterization compared with the traditional extrapolation, the final intensity of the model storm is increased by 10.5% (8.9%) in the maximum surface wind speed and by about 8.1 hPa (5.9 hPa) increase in the minimum sea surface pressure drop with (without) dissipative heating. This intensity increase is found to be mainly due to the reduced frictional dissipation in the surface layer with little to do with either the surface enthalpy flux or latent heat release in the eyewall convection.

The effect of the new surface roughness parameterization on the storm structure is found to be insignificant and occur only in the inner core region with the increase in tangential winds in the eyewall and the increase in temperature anomalies in the eye compared to the traditional extrapolation. This is because the difference in drag coefficient appears only in a small area under the eyewall. Consistent with previous findings, dissipative heating does increase the tropical cyclone intensity. We further show in this study as a byproduct that dissipative heating also affects the tropical cyclone inner core structure. It acts to shift the eyewall slightly inward and to reduce the outward slope of the eyewall. Although the dissipative heating acts to enlarge the intensity increase between the new and traditional surface roughness parameterizations, it reduces the difference in storm structure to some degree.

Note that our results are obtained from an atmospheric model with a constant sea surface temperature. The reduced surface wind stress may reduce the ocean upwelling and mixing, and thus reducing the SST cooling under the eyewall. Therefore, in a coupled model (as well in the real world), the intensity difference between the new and the traditional surface roughness parameterizations would be expected even larger than that found in this study. In addition, since the surface wind stress drives the storm surge in the coastal ocean, the storm surge would be overestimated if the wind stress were calculated based on the traditional extrapolation in a storm surge model. The use of the new observationally based surface roughness parameterization is therefore expected to improve the prediction of tropical cyclone structure and intensity, ocean waves, and storm surge by numerical models.

Finally, we should point out that the GPS dropwindsonde observations might be affected by the ocean waves, sea spray, and the horizontal movement of the dropsonde under the eyewall of tropical cyclones. These effects may have considerable impact on the accuracy of

calculations of the surface layer parameters as done by Powell et al. (2003). This can be inferred from the discrepancies between the drag coefficient given by Powell et al. (2003) and that obtained based on Fairall et al. (2003) for wind speed less than 25 m s^{-1}. Nevertheless, recent laboratory experiments (Alamaro et al. 2002; Donelan et al. 2004), theoretical consideration (Emanuel 2003; Mankin 2005), and the dropsonde observations (Drennan et al. 2007; French et al. 2007; Black et al. 2007) all converge to a transition at which the drag coefficient decreases with increasing wind speed for high wind speed. Although the main objective of this study is not to develop a new universal surface roughness parameterization scheme, the scheme that we have constructed can be used as an alternative to the traditional extrapolation in tropical cyclone models since it is more comparable to the best observations that we have had so far.

Future effort should be made to develop a new surface roughness parameterization scheme incorporating most available observations and test it in fully coupled atmosphere-wave-ocean models (Chen et al. 2007). In addition, as we mentioned in section 2 already, there could be considerable uncertainties in the current parameterization for exchange coefficient under hurricane winds since available observations are valid for surface wind speed up to 30-35 m s^{-1}. The nearly constant exchange coefficient does not warrant unchanged for higher winds since 30-35 m s^{-1} is just the transition for the drag coefficient from increasing to decreasing with surface winds speed. This should be investigated further once observational measurements for higher wind speed become available.

Note also that the effect of sea spray has not been considered in this study. Since we have known little about the sea spray source function under high wind conditions, current parameterizations are only experimental and include significant uncertainties as well. Our focus

in this study is on the effect of drag coefficient on the structure and intensity of the simulated tropical cyclones. The effect of sea spray needs to be investigated in the future once detailed observations for the sea spray generation under high wind conditions become available.

Acknowledgments: The authors are grateful to two anonymous reviewers for their thoughtful comments which helped improve our manuscript. The first author acknowledges the support by the National Basic Research Program of China (973 Program) (No. 2009CB421500), the National Natural Science Foundation of China under grants 40875039，and 40730948，and by the Typhoon Research Foundation of Shanghai Typhoon Institute/China Meteorological Administration under Grant 2006STB07 and 2008ST11.Wang has been supported by the U.S. Office of Naval Research under Grant N00014-021-0532, the National Science Foundation under Grant ATM-0427128, and the Frontier Research System for Global Change through its support to the International Pacific Research Center at the University of Hawaii.

REFERENCES

Alamaro, M., K.A. Emanuel, J. Colton, W. McGillis, and J.B. Edson, 2002: Experimental investigation of air-sea transfer of momentum and enthalpy at high wind speed. Preprints, *25th Conference on Hurricanes and Tropical Meteorology*, San Diego, CA, Amer. Meteor. Soc., 667-668.

Andreas, E.L., and K. Emanuel, 2001: Effects of sea spray on tropical cyclone intensity. *J. Atmos. Sci.*, **58**, 3741-3751.

Andreas, E.L., 2004: Spray Stress Revisited. *J. Phys. Oceanogr.*, **34**, 1429–1440.

Bao, J.-W., J.M. Wilczak, J.K. Choi, and L.H. Kantha, 2000: Numerical simulations of air-sea interaction under high wind conditions using a coupled model: A study of hurricane development. *Mon. Wea. Rev.*, **128**, 2190-2210.

Bister, M., and K.A. Emanuel, 1998: Dissipative heating and hurricane intensity. *Meteor. Atmos. Phys*., **65**, 233-240.

Black, P.G., E.A. D'Asaro, W.M. Drennan, J.R. French, P.P. Niiler, T.B. Sanford, E.J. Terrill, E.J. Walsh, and J.A. Zhang, 2007: Air-sea exchange in hurricanes: Synthesis of observations from the Coupled Boundary Layer Air-Sea Transfer experiment, *Bull. Amer. Meteor. Soc.*, **88**, 357-374.

Charnock, H., 1955: Wind stress on a water surface. *Q. J. Roy. Meteor. Soc*., **81**, 639-640.

Chen, Y., and M. K. Yau, 2001: Spiral bands in a simulated hurricane. Part I: vortex Rossby wave verification. *J. Atmos. Sci.*, **58**, 2128-2145.

Chen, S.S., J.F. Price, W. Zhao, M.A. Donelan, and E.J. Walsh, 2007: The CBLAST-hurricane program and the next-generation fully coupled atmosphere–wave–ocean models for hurricane research and prediction. *Bull. Amer. Meteor. Soc.*, **88**, 311–317.

Donelan, M.A., B.K. Haus, N. Reul, W.J. Plant, M. Stiassnie, H.C. Graber, O.B. Brown, and E.S. Saltzman, 2004: On the limiting aerodynamic roughness of the ocean in very strong winds. *Geophys. Res. Lett.,* **31,** L18306, doi:10.1029/2004GL019460.

Drennan, W.M., J. A. Zhang, J. R. French, C. McCormick, P.G. Black, 2007: Turbulent fluxes in the hurricane boundary layer. Part II: Latent heat flux. *J. Atmos. Sci.*, **64**, 1103-1115.

Durran, D.R., and J.B. Klemp, 1983: A compressible model for the simulation of moist mountain waves. *Mon. Wea. Rev*., **111**, 2341-2361.

Gray, W.M, E. Ruprecht, and R. Phelps, 1975: Relative humidity in tropical weather systems. *Mon. Wea. Rev*., **103**, 685-690.

Emanuel, K.A., 1995: Sensitivity of tropical cyclones to surface exchange coefficients and a revised steady-state model incorporating eye dynamics. *J. Atmos. Sci.*, **52**, 3969-3976.

Emanuel, K.A., 2003: A similarity hypothesis for air-sea exchange at extreme wind speeds. *J. Atmos. Sci*., **60**, 1420-1428.

Fairall, C.W., E.E. Bradley, J.E. Hare, A.A. Grachev, and J.B. Edson, 2003: Bulk parameterization of sir-sea fluxes: Updates and verification for the COARE algorithm. *J. Climate*, **16**, 571-591.

French, J.R., W.M., J.S. Zhang, and P.G. Black, 2007: Turbulent fluxes in the hurricane boundary layer: Part I: Momentum flux. *J. Atmos. Sci*., **64**, 1089-1102.

Kurihara, Y., M.A. Bender, R.E. Tuleya, and R.J. Ross, 1998: The GFDL hurricane prediction system and its performance in the 1995 hurricane season. *Mon. Wea. Rev*., **126**, 1306-1322.

Large, W.C., and S. Pond, 1981: Open ocean momentum flux measurements in moderate to strong winds. *J. Phys. Oceanogr*., **11**, 324-336.

Liu, T., K.B. Katsaros, and J.A. Businger, 1979: Bulk parameterization of air-sea exchanges of heat and water vapor including the molecular constraints at the interface. *J. Atmos. Sci*., **36**, 1722-1735.

Malkus, J.S., and H. Riehl, 1960: On the dynamics and energy transformations in steady-state hurricanes. *Tellus*, **12**, 1-20.

Makin, V. K., 2005: A note on the drag of the sea surface at hurricane winds. *Tellus，Bound.-Layer Meteor.,* **115**,169–176.

Montgomery M. T., R. J. Kallenbach: 1997, A theory for vortex Rossby-waves and its application to spiral bands and intensity changes in hurricanes. *Quart. J. Roy. Meteor. Soc.* **123**, 435–465.

——, C. Lu: 1997, Free waves on barotropic vortices. Part I: Eigenmode structure. *J. Atmos. Sci.*, **54**, 1868–1885.

——, J. Enagonio: 1998, Tropical cyclogenesis via convectively forced vortex Rossby waves in a three dimensional quasigeostrophic model. *J. Atmos. Sci.*, **55**, 3176–3207.

——, G. Brunet: 2002, Vortex Rossby waves on smooth circular vortices. Part II: Idealized numerical experiments for tropical cyclone and polar vortex interiors. *Dyn. Atmos. Oceans,* **35**, 179–204.

Moon, I.-J., T. Hara, I. Ginis, S. E. Belcher, and H. Tolman, 2004a: Effect of surface waves on air–sea momentum exchange. Part I: Effect of mature and growing seas. *J. Atmos. Sci.,* **61,** 2321–2333.

——, I. Ginis, and T. Hara, 2004b: Effect of surface waves on air–sea momentum exchange.

Part II: Behavior of drag coefficient under tropical cyclones. *J. Atmos. Sci.,* **61,** 2334–2348.

——, ——, and ——, 2004c: Effect of surface waves on Charnock coefficient under tropical cyclones. *Geophys. Res. Lett.,* **31,** L20302, doi:10.1029/2004GL020988.

Ooyama, K., 1969: Numerical simulation of the life cycle of tropical cyclones. *J. Atmos. Sci*., **26**, 3-40.

Powell, M.D., P.J. Vickery, and T.A. Reinhold, 2003: Reduced drag coefficient for high wind speeds in tropical cyclones. *Nature*, **422**, 279-283.

Rotunno, R., and K. Emanuel, 1987: An air-sea interaction theory for tropical cyclones. Part II: Evolutionary study using a non-hydrostatic axisymmetric model. *J. Atmos. Sci.*, **44,** 542-561.

Smith, S.D., 1988: Coefficients for sea surface wind stress, heat, and wind profiles as a function of wind speed and temperature. *J. Geophys. Res*., **93**, 15,467-15,472.

Wang, Y., 1996: On the forward-in-time upstream advection scheme for non-uniform and time-dependent flow. *Meteor. Atmos. Phys.*, **61**, 27-38.

Wang, Y., 1999: A triply-nested movable mesh tropical cyclone model with explicit cloud microphysics-TCM3. *BMRC report* No. **74**. Bureau of Meteorology Research Center, Australia.

Wang, Y., 2001: An explicit simulation of tropical cyclones with a triply nested movable mesh primitive equation model: TCM3. Part I: Model description and control experiment. *Mon. Wea. Rev*., **129**, 1370-1394.

Wang, Y., 2002a: An explicit simulation of tropical cyclones with a triply nested movable mesh primitive equation model: TCM3. Part II: Some model refinements and sensitivity to cloud microphysics parameterization. *Mon. Wea. Rev*. **130**, 3022-3036.

Wang, Y., 2002b: Vortex Rossby waves in a numerically simulated tropical cyclone. Part I: Overall structure, potential vorticity and kinetic energy budgets. *J. Atmos. Sci.,* **59**, 1213-1238.

Wang, Y., 2002c: Vortex Rossby waves in a numerically simulated tropical cyclone. Part II: The role in tropical cyclone structure and intensity changes. *J. Atmos. Sci.,* **59**, 1239-126.

Wang, Y., 2007: A multiply nested, movable mesh, fully compressible, nonhydrostatic tropical cyclone model – TCM4: Model description and development of asymmetries without explicit asymmetric forcing. *Meteor. Atmos. Phys*., **97**, 93-116.

Wang, Y., J.D. Kepert, and G.J. Holland, 2001: The effect of sea spray evaporation on tropical cyclone boundary layer structure and intensity. *Mon. Wea. Rev.*, **129**, 2481-2500.

Wang, Y., and C.-C. Wu, 2004: Current understanding of tropical cyclone structure and intensity changes–A review. *Meteor. Atmos. Phys*., **87**, 257-278.

Wicker, L.J., and W.C. Skamarock, 2002: Time-spitting scheme for elastic models using forward time schemes, *Mon. Wea. Rev*., **130**, 2088-2097.

Yang, B., Y. Wang, and B. Wang, 2007: The effect of internally generated inner core asymmetric structure on tropical cyclone intensity. *J. Atmos. Sci.*, **64**, 1165-1188.

Zhang, D-L, and E. Altshuler, 1999: The effect of dissipative heating on hurricane intensity. *Mon. Wea. Rev.*, **127**, 3032-3038.

Zhang, J.A., P.G. Black, J.R. French, and W.M. Drennan, 2008: First direct measurements of enthalpy flux in the hurricane boundary layer: The CBLAST results, *Geophys. Res. Lett.*, **35**, L14813, doi:10.1029/2008GL034374.

Figure Caption

Figure 1. The surface friction velocity (a), surface roughness length (b), drag and exchange coefficients (c), and the parameter $(C_h/C_d)^{1/2}$ (d) as a function of wind speed at neutral surface condition. The solid curves are for the traditional use of extrapolation for high wind speed; dashed curves are for the new parameterization constructed in this study. The open circles indicate the middle values and the corresponding vertical bars represent the ranges of estimates based on 95% confidence limits from GPS dropsonde observations, reproduced from Powell et al. (2003).

Figure 2. The evolution of the maximum wind speed at the lowest model level (35.6 m above the sea surface, upper panels) and the minimum central sea surface pressure (lower panels) in the four experiments listed in Table 1. Note that DH denotes dissipative heating.

Figure 3. The radial profiles of the azimuthal mean 10-m height wind speed (upper panels) and rainfall rate (lower panels) averaged between 144 and 216 h of simulations in the four experiments listed in Table 1.

Figure 4. The radial profiles of the azimuthal mean surface momentum roughness length (upper panels) and friction velocity (lower panels) averaged between 144 and 216 h of simulations in the four experiments listed in Table 1.

Figure 5. The radial profiles of the azimuthal mean surface drag (Cd) and exchange (Ch) coefficients (upper panel) and the parameter $(C_h/C_d)^{1/2}$ averaged between 144 h and 216 h of simulations in the four experiments listed in Table 1.

Figure 6. The radial profiles of the azimuthal mean surface enthalpy flux (upper panels) and surface wind stress (lower panels) averaged between 144 h and 216 h of simulations in the four experiments listed in Table 1.

Figure 7. The axisymmetric structure of the simulated tropical cyclone in the experiments with the traditional surface roughness parameterization and dissipative heating (CTL_DH) averaged between 144 h and 216 h of simulation. Shown are (a) tangential wind (m s^{-1}), (b) radial wind (m s^{-1}); (c) vertical velocity (m s^{-1}), (d) temperature anomaly (K), (e) potential vorticity (PVU, 1 PVU=10^{-6} K m^2 kg s^{-1}), and (f) eddy kinetic energy (m^2 s^{-2}). Contour intervals are 10 m s^{-1} in (a), 2.5 m s^{-1} in (b), 0.5 m s^{-1} in (c), 2 K in (d), 10 PVU in (e), and 3 m^2 s^{-2} in (f).

Figure 8. As in Figure 7, but for experiment NEW_DH in Table 1.

Figure 9. The difference in the axisymmetric structure averaged during a 72 h period from 144 h to 216 h of simulation between two storms from the experiments NEW_DH and CTL_DH listed in Table 1. Shown are (a) tangential wind (m s^{-1}), (b) radial wind (m s^{-1}); (c) vertical velocity (m s^{-1}), (d) temperature anomaly (K), (e) potential vorticity (PVU), and (f) eddy kinetic energy (m^2 s^{-2}). Contour intervals are 1 m s^{-1} in (a), 0. 25 m s^{-1} in (b), 0.2 m s^{-1} in (c), 0.5 K in (d), 5 PVU in (e), and 1 m^2 s^{-2} in (f).

Figure 10. Azimuthal mean dissipative heating (K h^{-1}) averaged between 144 h and 216 h of simulation in (a) CTL_DH, (b) NEW_DH, and (c) the difference between NEW_DH and CTL_DH. Contour intervals are 1 K h^{-1} in (a) and (b) and 0.5 K h^{-1} in (c).

Figure 11. As in Figure 9 but for the difference between two storms in the experiments NEW_noDH and CTL_noDH listed in Table 1.

Figure 12. As in Figure 9 but for the difference between two storms in the experiments CTL_DH and CTL_noDH listed in Table 1. Note that contour interval is 0.5 m s^{-1} in (b).

Table 1. Summary of the four experiments performed to evaluate the effect of surface roughness parameterization and dissipative heating on the model storm structure and intensity in this study. Note that the peak intensity averaged in the last 3 days (144-216 h) in each experiment is given in the last column in the table.

Experiment	Surface roughness parameterization	Dissipative heating	Peak storm intensity	
			Vmax (m s^{-1})	Pmin (hPa)
CTL_DIS	Traditional scheme	Yes	73.3	914.0
NEW_DIS	New scheme	Yes	81.0	905.9
CTL_noDIS	Traditional scheme	No	70.6	920.3
NEW_noDIS	New scheme	No	76.9	914.4

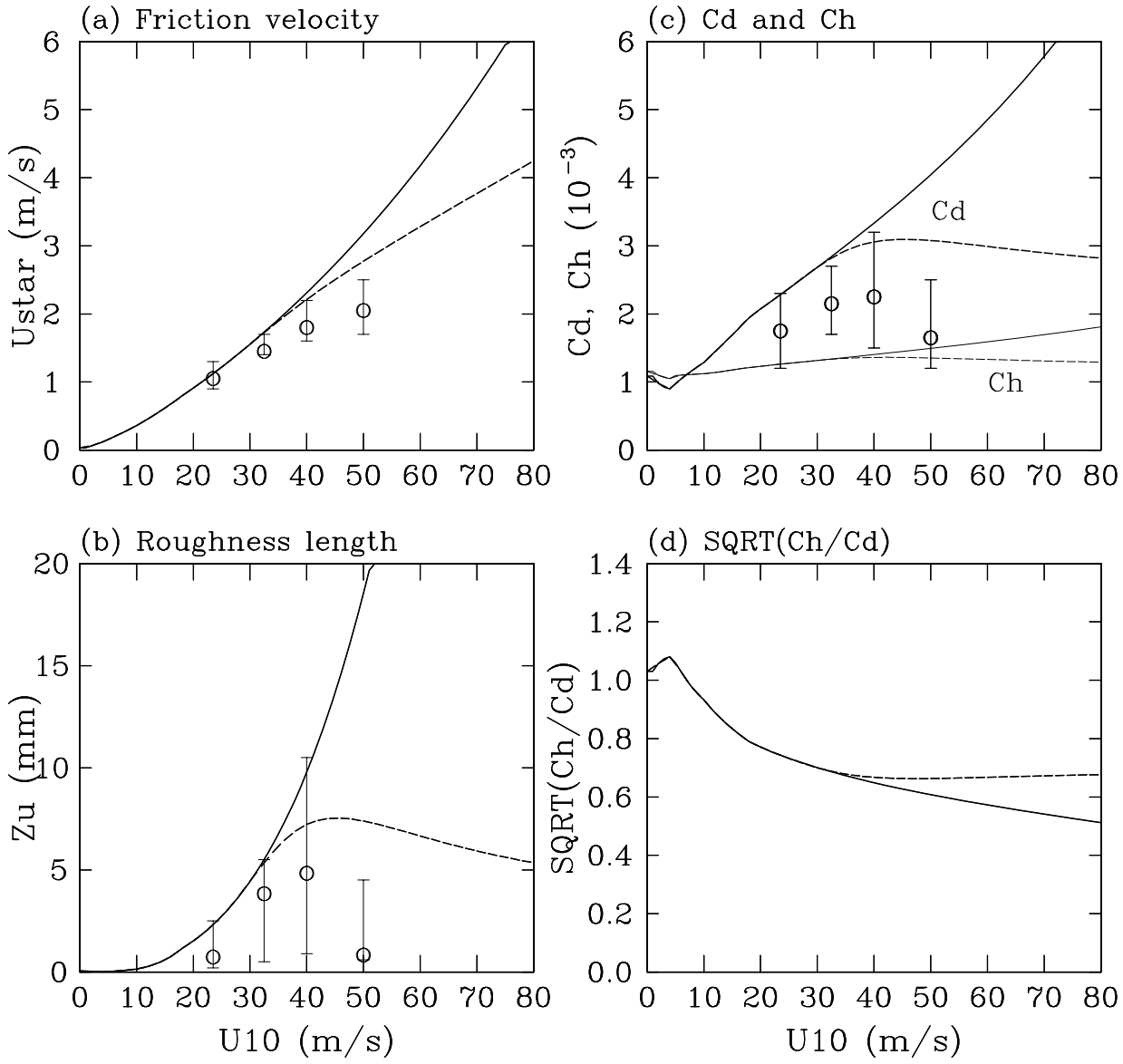

Figure 1. The surface friction velocity (a), surface roughness length (b), drag and exchange coefficients (c), and the parameter $(C_h/C_d)^{1/2}$ (d) as a function of wind speed at neutral surface condition. The solid curves are for the traditional use of extrapolation for high wind speed; dashed curves are for the new parameterization constructed in this study. The open circles indicate the middle values and the corresponding vertical bars represent the ranges of estimates based on 95% confidence limits from GPS dropsonde observations, reproduced from Powell et al. (2003).

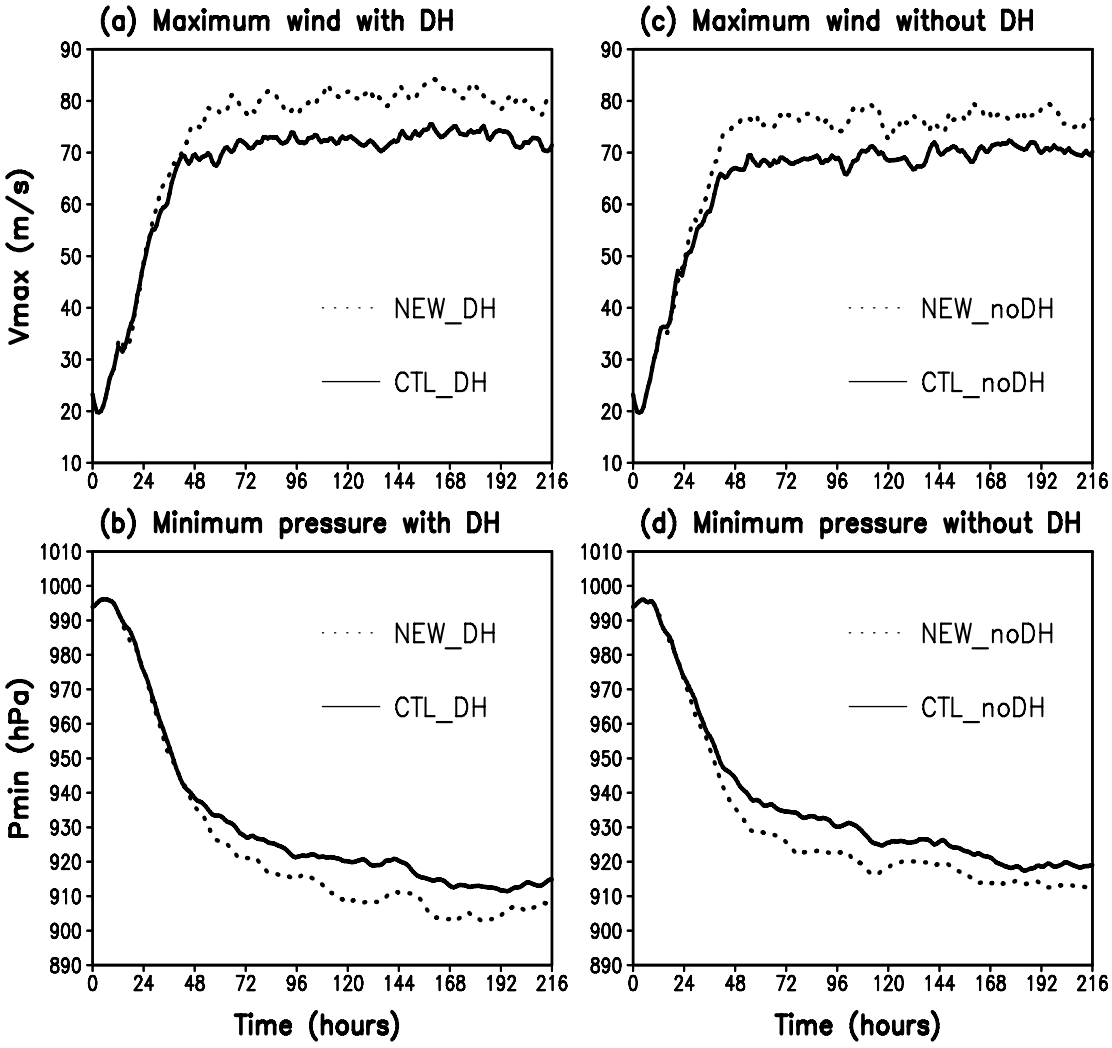

Figure 2. The evolution of the maximum wind speed at the lowest model level (35.6 m above the sea surface, upper panels) and the minimum central sea surface pressure (lower panels) in the four experiments listed in Table 1. Note that DH denotes dissipative heating.

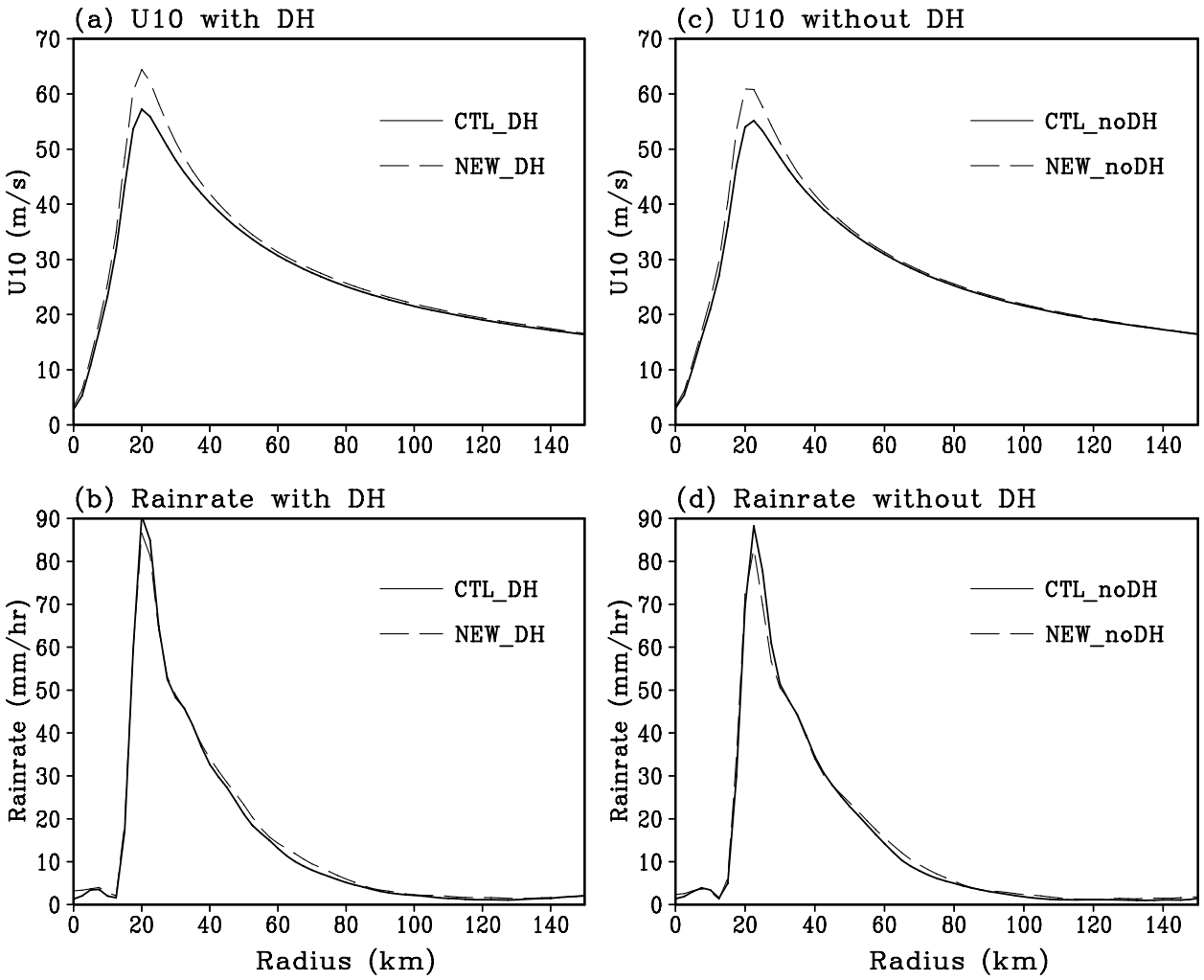

Figure 3. The radial profiles of the azimuthal mean 10-m height wind speed (upper panels) and rainfall rate (lower panels) averaged between 144 and 216 h of simulations in the four experiments listed in Table 1.

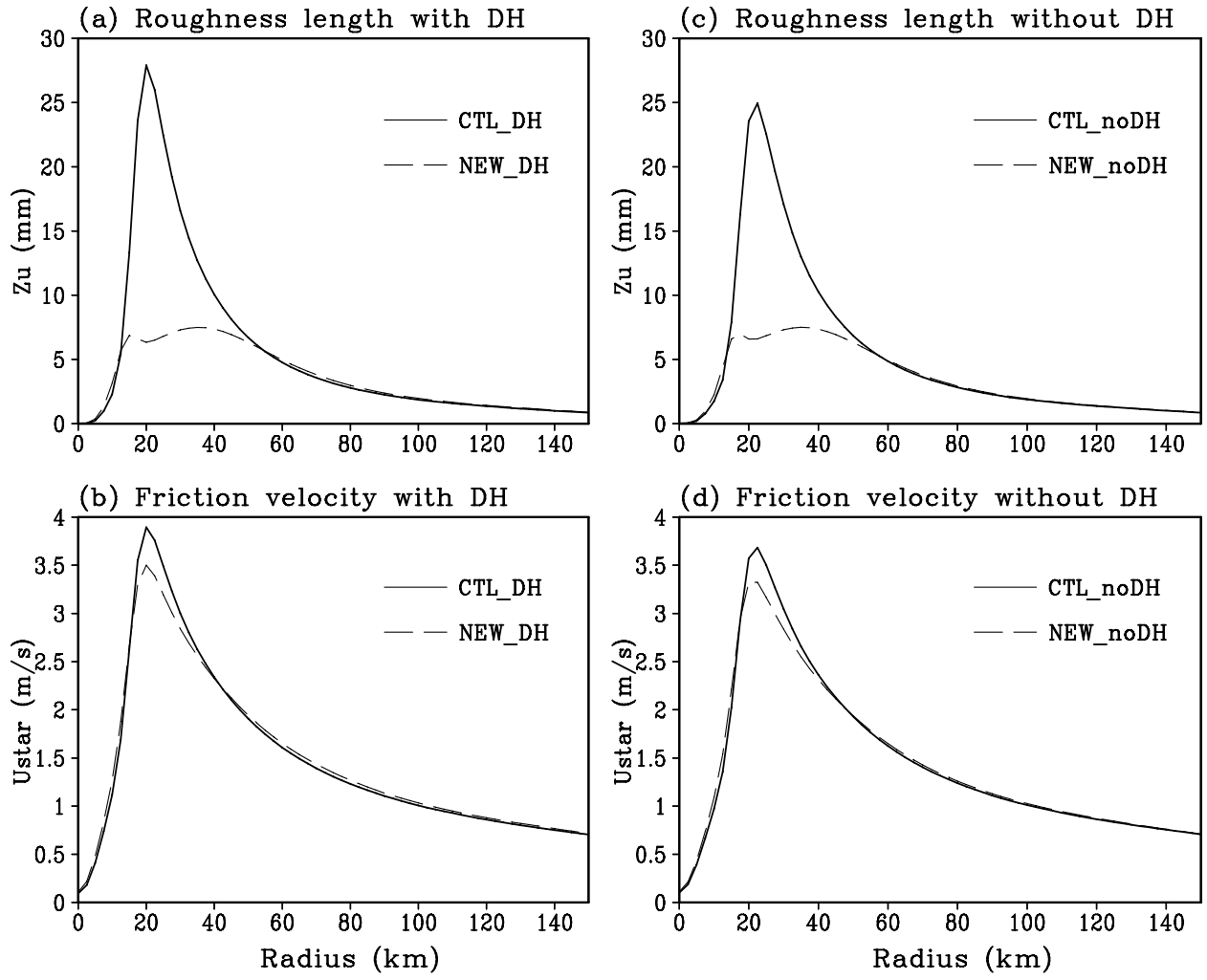

Figure 4. The radial profiles of the azimuthal mean surface momentum roughness length (upper panels) and friction velocity (lower panels) averaged between 144 and 216 h of simulations in the four experiments listed in Table 1.

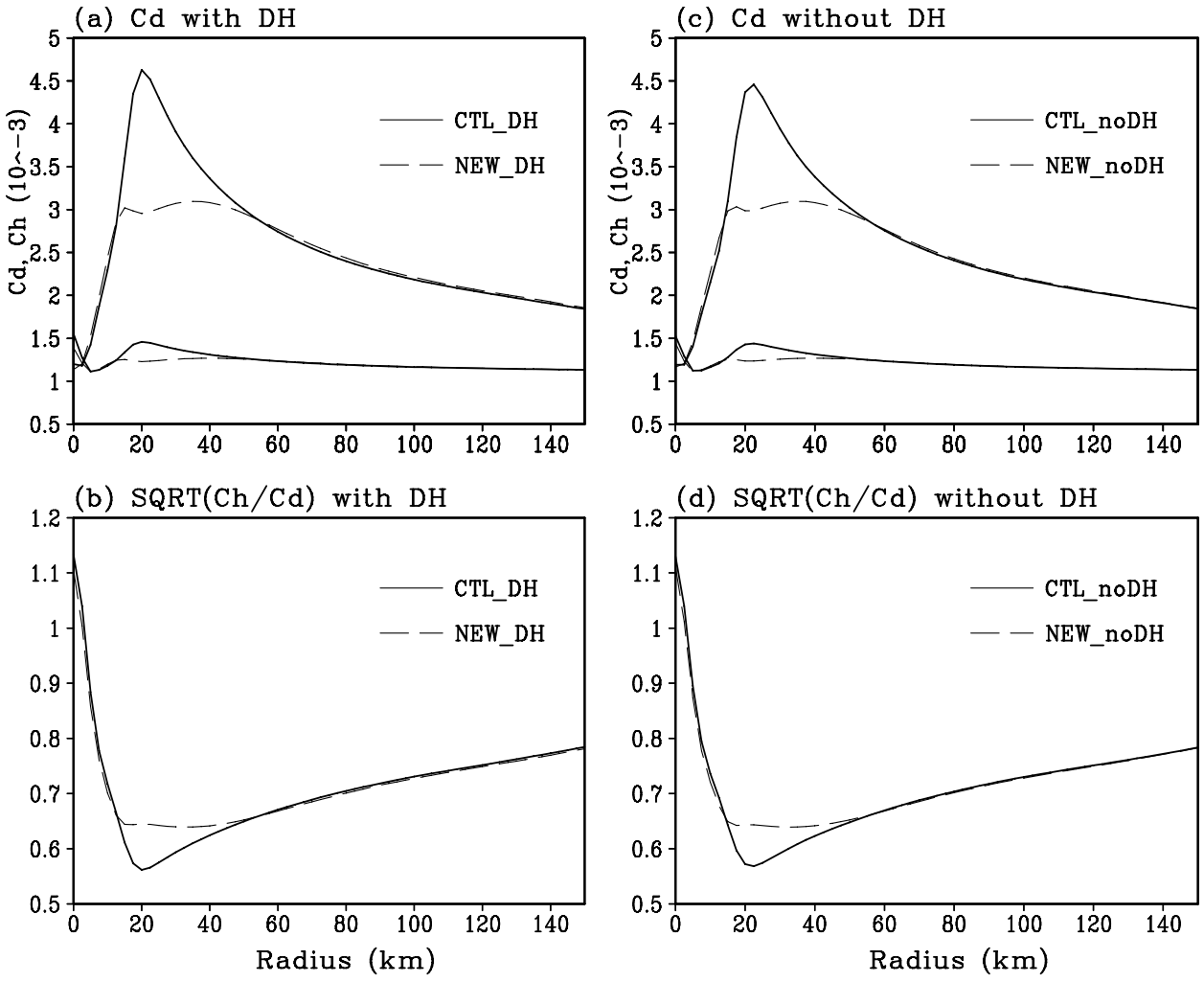

Figure 5. The radial profiles of the azimuthal mean surface drag (Cd) and exchange (Ch) coefficients (upper panel) and the parameter $(C_h/C_d)^{1/2}$ averaged between 144 h and 216 h of simulations in the four experiments listed in Table 1.

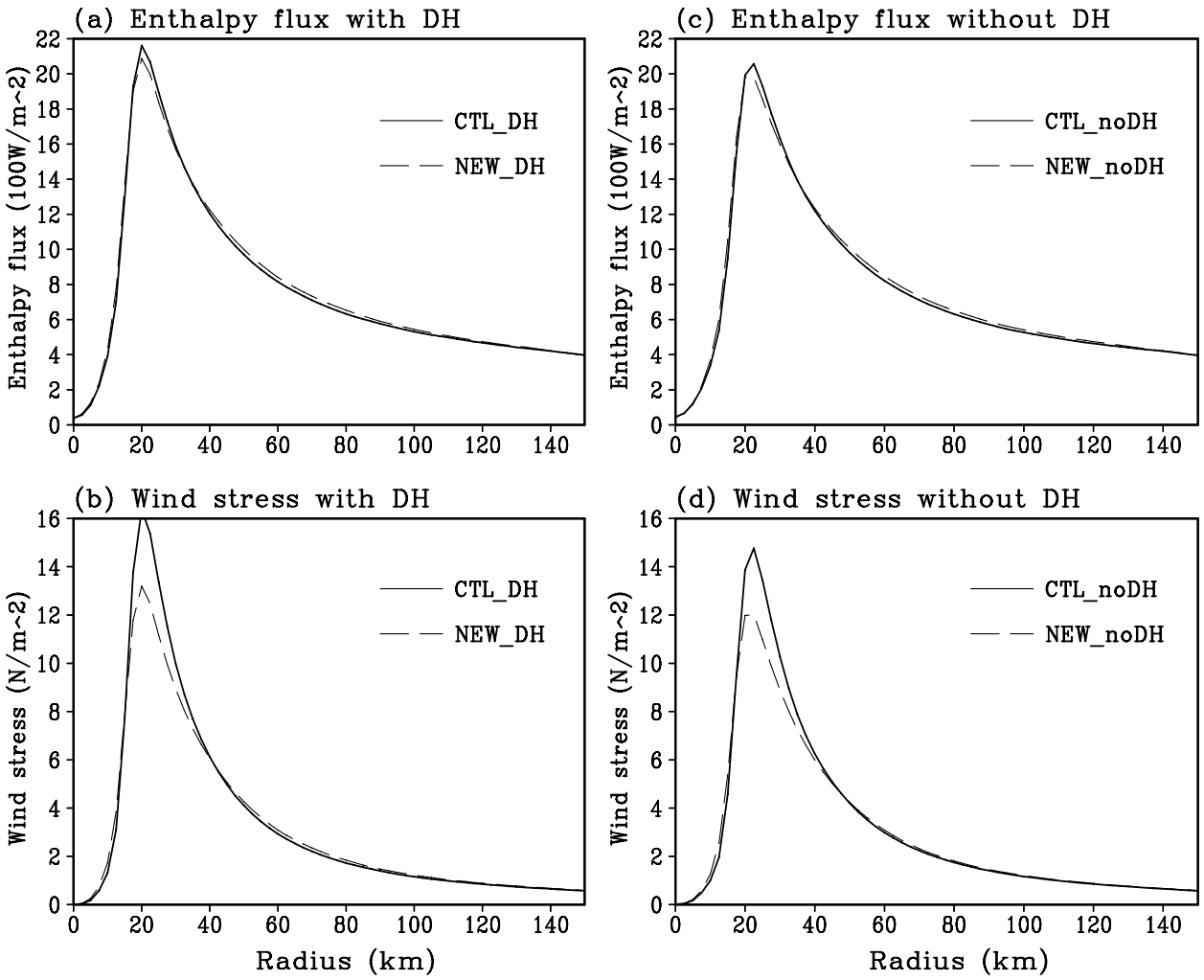

Figure 6. The radial profiles of the azimuthal mean surface enthalpy flux (upper panels) and surface wind stress (lower panels) averaged between 144 h and 216 h of simulations in the four experiments listed in Table 1.

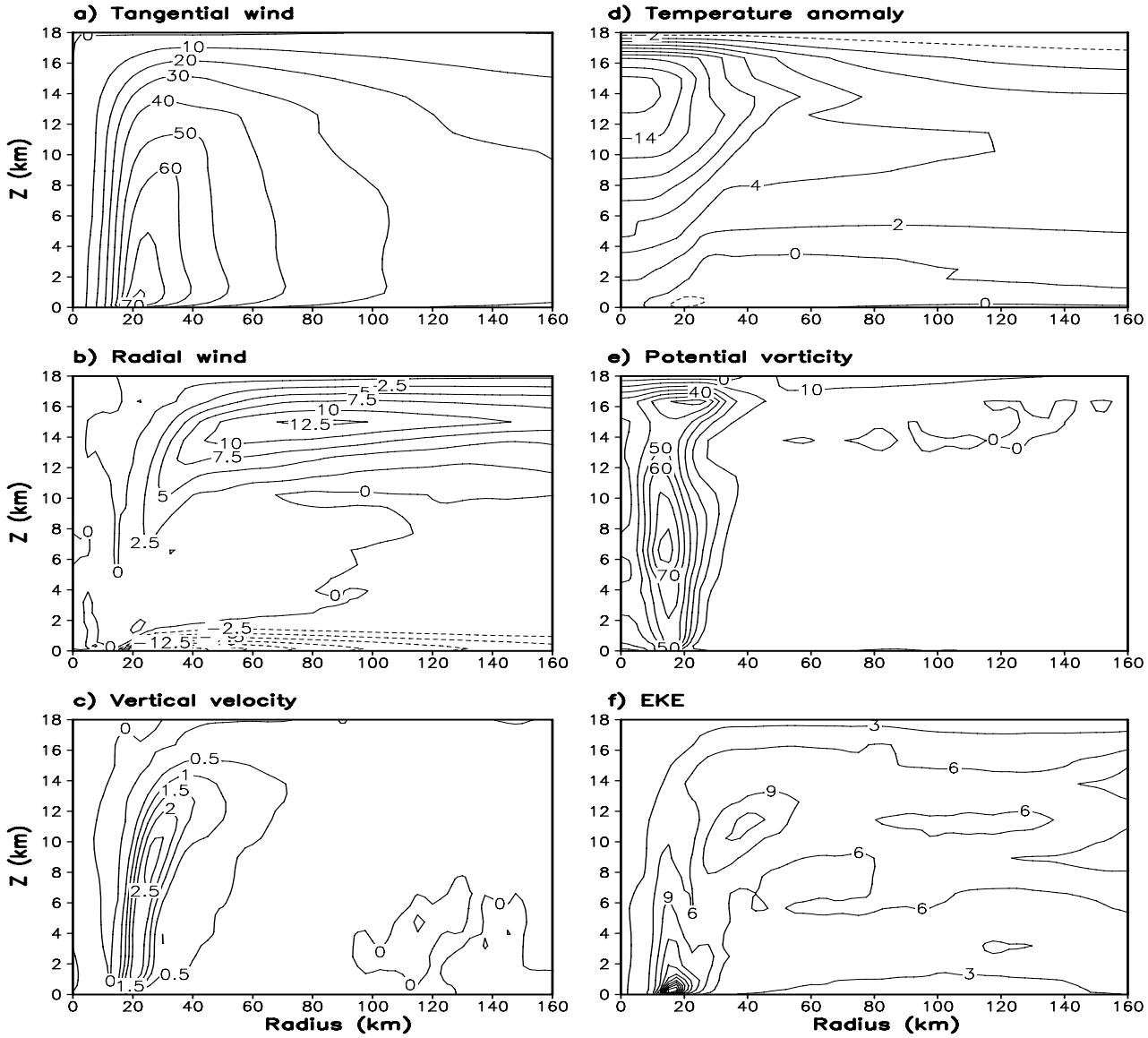

Figure 7. The axisymmetric structure of the simulated tropical cyclone in the experiments with the traditional surface roughness parameterization and dissipative heating (CTL_DH) averaged between 144 h and 216 h of simulation. Shown are (a) tangential wind (m s^{-1}), (b) radial wind (m s^{-1}); (c) vertical velocity (m s^{-1}), (d) temperature anomaly (K), (e) potential vorticity (PVU, 1 PVU=10^{-6} K m^2 kg s^{-1}), and (f) eddy kinetic energy (m^2 s^{-2}). Contour intervals are 10 m s^{-1} in (a), 2.5 m s^{-1} in (b), 0.5 m s^{-1} in (c), 2 K in (d), 10 PVU in (e), and 3 m^2 s^{-2} in (f).

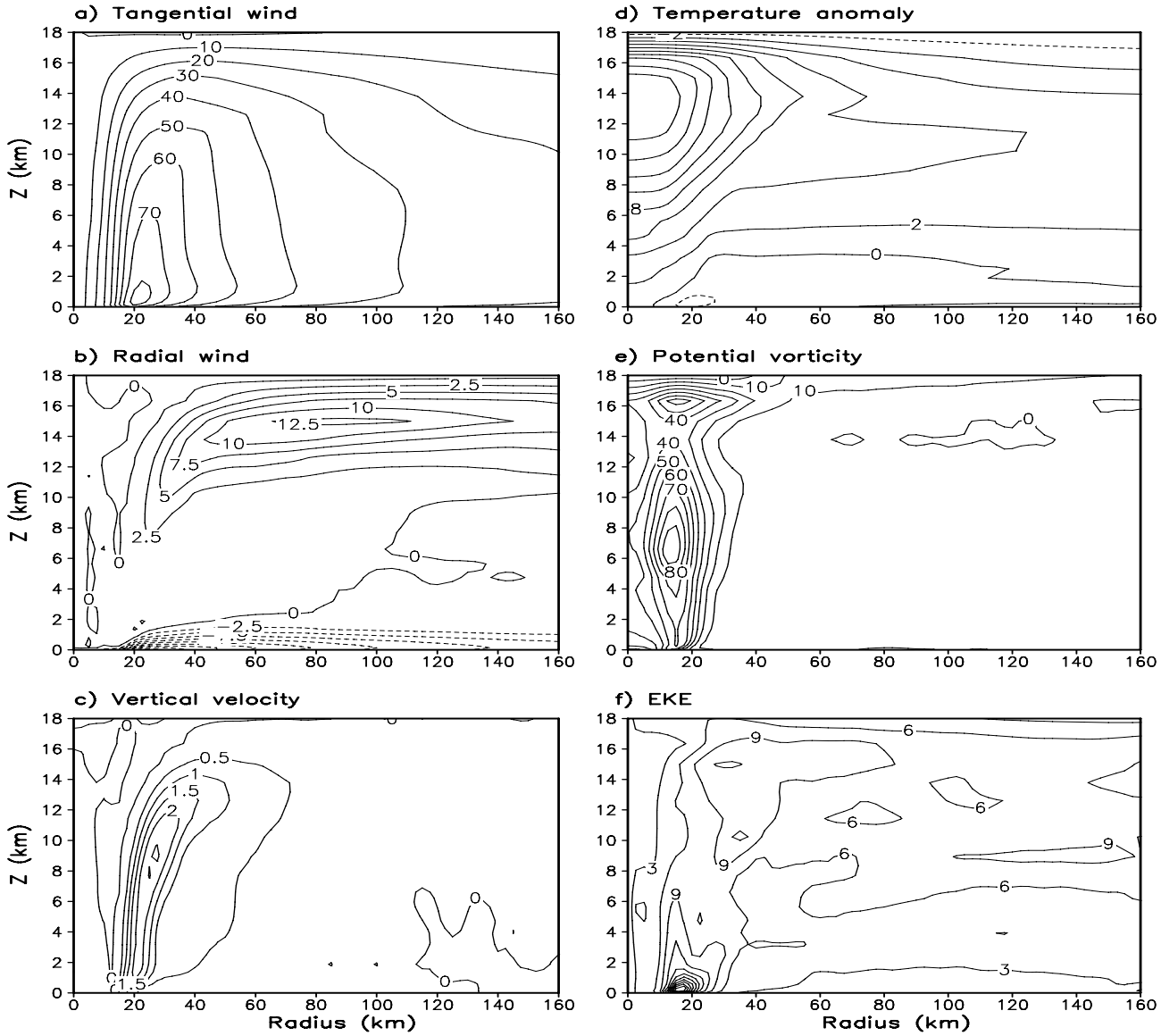

Figure 8. As in Figure 7, but for experiment NEW_DH in Table 1.

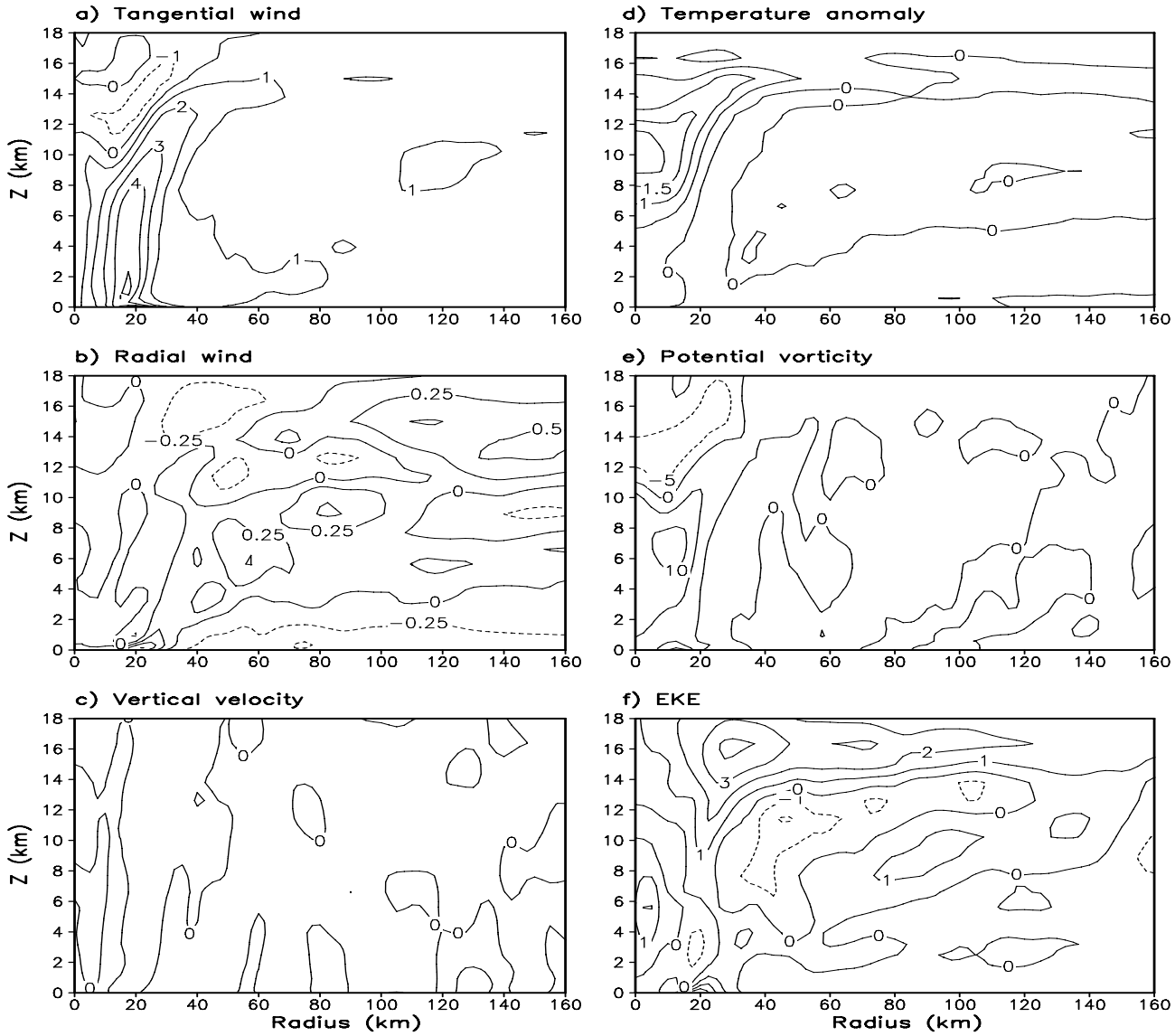

Figure 9. The difference in the axisymmetric structure averaged during a 72 h period from 144 h to 216 h of simulation between two storms from the experiments NEW_DH and CTL_DH listed in Table 1. Shown are (a) tangential wind (m s^{-1}), (b) radial wind (m s^{-1}); (c) vertical velocity (m s^{-1}), (d) temperature anomaly (K), (e) potential vorticity (PVU), and (f) eddy kinetic energy (m^2 s^{-2}). Contour intervals are 1 m s^{-1} in (a), 0. 25 m s^{-1} in (b), 0.2 m s^{-1} in (c), 0.5 K in (d), 5 PVU in (e), and 1 m^2 s^{-2} in (f).

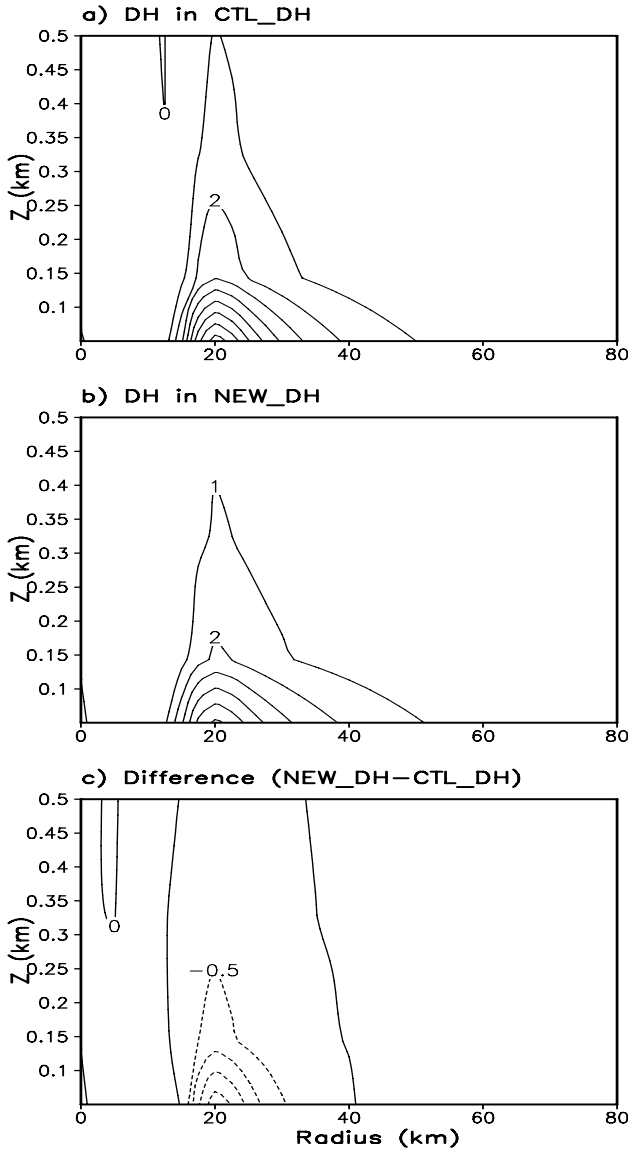

Figure 10. Azimuthal mean dissipative heating (K h^{-1}) averaged between 144 h and 216 h of simulation in (a) CTL_DH, (b) NEW_DH, and (c) the difference between NEW_DH and CTL_DH. Contour intervals are 1 K h^{-1} in (a) and (b) and 0.5 K h^{-1} in (c).

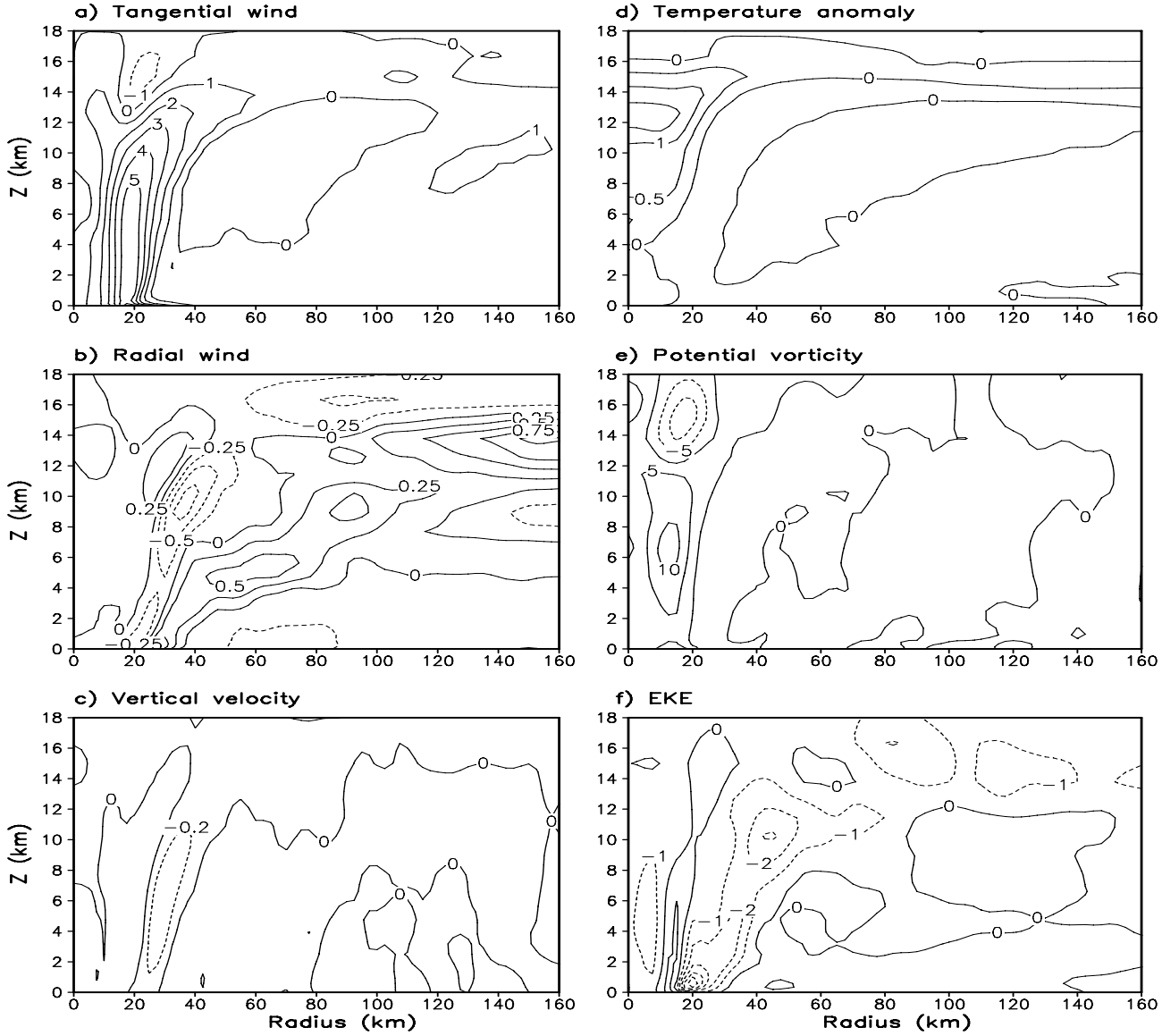

Figure 11. As in Figure 9 but for the difference between two storms in the experiments NEW_noDH and CTL_noDH listed in Table 1.

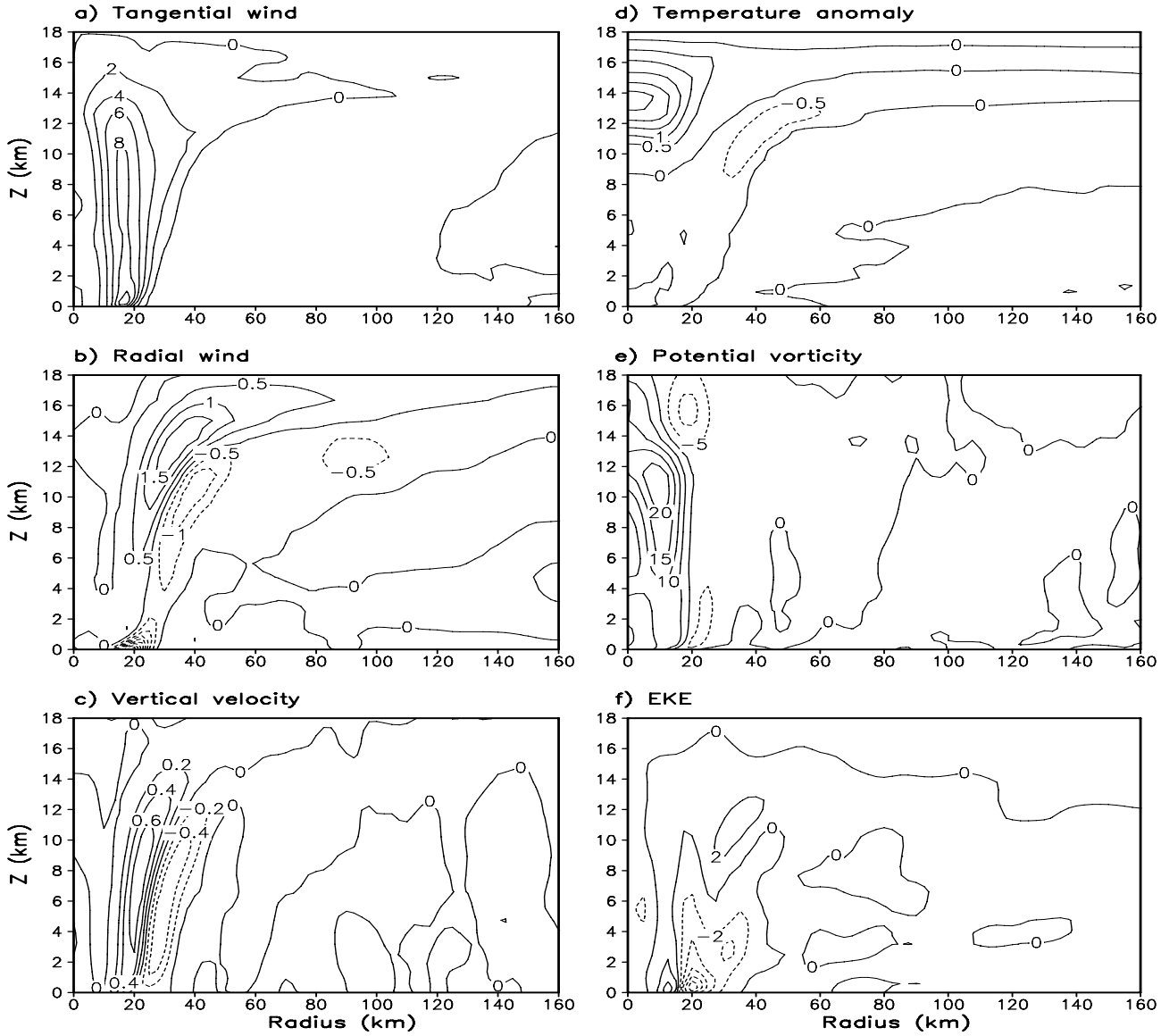

Figure 12. As in Figure 9 but for the difference between two storms in the experiments CTL_DH and CTL_noDH listed in Table 1. Note that contour interval is 0.5 m s^{-1} in (b).